AFOSR No. [illegible]
Contract No. AF49(638)-165
Project No. 9751

(10)

A SPRAY COMBUSTION MODEL WITH DROPLET BREAKUP INCLUDING GAS DYNAMIC COUPLING

By

S. Burstein, S. Hammer, V.D. Agosta

June 1961

POLYTECHNIC INSTITUTE OF BROOKLYN

DEPARTMENT OF
MECHANICAL ENGINEERING

A SPRAY COMBUSTION MODEL WITH DROPLET BREAKUP INCLUDING GAS DYNAMIC COUPLING

By

Samuel Z. Burstein, Sanford S. Hammer and

Vito D. Agosta

ABSTRACT

A simplified model is proposed for the combustion of a bi-propellant spray. The model considers two subsystems: one the spray, the other, combusted gases. These subsystems are coupled together by heat transfer, mass transfer and momentum transfer. The solution of the problem relies upon the integration of a system of seven nonlinear differential equations. The integration is performed using the IBM 704 digital computer. It appears that under the given boundary conditions a co-operative evaporation process occurs, in which increased velocity gradients cause increased evaporation which increases the velocity gradient.

A series of tests have been made on a two inch diameter, variable length rocket motor, using JP-5A and liquid oxygen. A simple converging diverging nozzle is employed to give high chamber exit Mach numbers (.4 to .5). For a given set of injection parameters, under stable operating conditions, the results indicate that the steepest portion of the gradient, which corresponds to evaporation of the major portion of the fuel, is always found in a fixed region of the chamber, independent of the absolute length of the chamber. The experimental results appear to be in agreement with the theory for the conditions investigated.

INTRODUCTION

The processes involved in the combustion phenomena in a liquid propellant rocket consist of spraying of fuel and oxidizer into the chamber, mixing, evaporation of the droplets, interdiffusion of the vapors, and then the chemical reaction. The chain of events stated here is still an oversimplified version of the true account. The overall process is so complex that we must resort to the study of simplified models having some of the most important features of the real physical phenomena. In the evaporation and combustion of a spray, we simplify to a point where we discuss the ballistics, evaporation and combustion of individual droplets of fuel. If we assume that interaction between single droplets is negligible, then evaporation rates of a distribution of droplets are additive. Thus, a distribution of droplets can be used to approximate the evaporation rates of certain spray configurations.

This paper depicts combustion in a rocket motor as controlled by the evaporation process of an arbitrary number of droplets of injected fuel. The evaporation rate of the droplet of fuel is of course most affected by its immediate environment, which in this case happens to be high velocity gases at temperatures in the range of 5800°R, and at a pressure of approximately 11 atmospheres. The environment is determined, to a large extent, by the rate of evaporation of the droplet of fuel, that is, by the rate at which chemical energy is added to the system. Thus, there is a strongly coupled system consisting of the evaporation processes and the fluid dynamics of the environment. The results of the evaporation of the droplets of fuel are weighted to yield a mass rate of flow which is consistent with approximately a 500 pound thrust chamber.

THE DROPLET MODEL

The evaporation of a spray is treated as the summation of the evaporation of individual drops. The general reliability of droplet drag and vaporization rate correlations for single droplets, when applied to sprays, is suspect. This work is aimed at determining the consequences of the assumption of additivity of droplets.

Liquid: The liquid is completely mixed; has a uniform temperature, and its composition, vapor pressure, surface tension, specific heat, and viscosity is that of JP-5; the vapor pressure, surface tension, specific heat and viscosity are taken as functions of temperature.

Film: The film consists of two components: (a) with properties of JP-5A, and (b) with properties averaged between carbon dioxide and water vapor, including average critical pressure and temperature.

Outer Boundary of Film: The film boundary temperature is that of the bulk gas; where the temperature and pressure of bulk gas vary in a prescribed manner (from the hydrodynamic calculations): the partial pressure of the hydrocarbons equals zero and the partial pressure of the inert component equals the total pressure.

Bulk Gas: The bulk gas temperature, pressure and velocity are determined by fluid dynamic calculations. Its composition is determined by assuming that all of the oxidizer is vaporized and that chemical equilibrium exists between the vaporized hydrocarbons and the oxidizer.

Inner Boundary of the Film: The inner boundary temperature is that of the liquid where the partial pressure of the hydrocarbon equals the vapor pressure and the partial pressure of the combustion products equals the total pressure minus the partial pressure of the hydrocarbon.

Heat Transfer: The heat transfer process is assumed to be by convection only where the correlation of Ranz and Marshall (1) [5] is used.

$$(Nu)_h = \frac{2hr}{K_m} = 2 + 0.6\ Pr^{1/3}\ Re^{1/2} \qquad (1)$$

r, droplet radius, ft.

h, film coefficient, BTU/ft^2-sec-deg. F

K_m, mean film conductivity, BTU/ft-sec-deg F

Pr, Prandtl number, dimensionless = $\frac{C_p\ \mu}{K}$

Re, Reynolds number, dimensionless = $\frac{2r\ (u-v)\rho}{\mu}$

A correction is made for sensible heat carried by the evaporating fuel moving away from the drop, (6)

$$q_v = hA_L\ (T_G - T_L)\ Z \qquad (2)$$

Here q_v is the heat in BTU per second absorbed by the droplet by convection; A_L is the area of the droplet in square feet, and T_g and T_L are the gas and droplet temperatures, respectively. Z is defined by

$$Z = \frac{\beta}{e^{\beta} - 1} \qquad \beta = \frac{\dot{W}\ C_p}{h\ A_L}$$

It is seen then, that Z is that fraction of total heat transfer from the gas that arrives at the surface of the liquid drop. β is dimensionless since W is the vapor from the evaporating drop in pounds per second, and C_p is the specific heat at constant pressure of the vapor in BTU/lb ^{o}F.

---

[5] Numbers in parentheses indicate references at end of paper.

The temperature charge may then be computed, since λ, the latent heat of the drop (BTU/lb) is known. If θ is the time in seconds, then

$$\frac{d T_L}{d \theta} = \frac{q_L}{C_L M_L} \qquad (3)$$

where q_L, the net heat absorbed by the evaporating droplet, is given by

$$q_L = q_v - \dot{W} \lambda$$

C_L is the specific heat of the liquid (BTU/lb$^\circ$F) and M_L is the weight of the liquid drop in pounds.

Mass Transfer is assumed to be by film diffusion. Here thermal diffusion (the Dufour Effect) is neglected and the correlation of Ranz and Marshall (1) is used:

$$(Nu)_w = \frac{2 K_g r}{D_v M_g / R} = 2 + 0.6 \, Sc^{1/3} Re^{1/2} \qquad (4)$$

where N_u, Nusselt number, dimensionless

D_v, diffusivity, ft^2/sec

M_g, molecular weight of fuel vapor, lb/lb-mole

R, gas constant, ft-lb/lb-mole $^\circ$R

Sc, Schmidt number, dimensionless $= \frac{\mu}{D_v \rho}$

The diffusivity is calculated by the equation given by Bird (2)

$$D_v = \frac{(P_{ca}\, P_{cb})^{1/3} (T_{ca}\, T_{cb})^{5/12}}{\left(\frac{2\, M_a\, M_b}{M_a + M_b}\right)^{1/2}} \quad \frac{a^*}{p}\, T_R^{\,b} \qquad (5)$$

molecular diffusion coefficient

Here

$$T_R = \frac{\bar{T}}{(T_{ca}\, T_{cb})^{1/2}}$$

P_{ca} is the pseudo-critical pressure of JP-5A, atmospheres

P_{cb} is the average critical pressure of CO_2 and H_2O, atm.

$\bar{T}$ is the average temperature of liquid droplet and combustion products, ^oR

T_{ca} is the pseudo-critical temperature of JP-5A, ^oR

T_{cb} is an average critical temperature of CO_2 and H_2O, ^oR

while a' is a correlation constant = 3.882×10^4

and b is a correlation constant = 1.8229

M_a is the molecular weight of JP-5A, lb/lb-mole

and M_b is the average molecular weight of CO_2 and H_2O, lb/lb-mole

A correction is made for the effect of bulk motion of the fluid away from the evaporating interface (3). If P_L is the vapor pressure of the liquid fuel, and p the total static pressure of the gases, then

$$\dot{W} = K_g\, A_L P_L \alpha \qquad (6)$$

where

$$\alpha = \frac{P}{P_L} \ln \frac{P}{P-P_L} \qquad (7)$$

α is a correction factor to account for the unidirectional diffusion process rather than just considering the equimolal diffusion transfer coefficient K_g which is computed from equation 4.

The change in radius of the fuel drop in time can be calculated if the liquid density ρ_L is known as a function of the drop temperature. The continuity equation for the liquid drop is:

$$\frac{d(\rho V')}{d\theta} = -\dot{W}$$

v' is the drop volume $= \frac{4}{3}\pi r^3$

$$\boxed{\frac{dr}{d\theta} = -\frac{\dot{W}}{A_L \rho_L} - \frac{r}{3\rho_L}\left(\frac{d\rho_L}{dT_L}\right)\frac{dT_L}{d\theta}} \qquad (8)$$

<u>Drag</u> is calculated from Ingebo's correlation on liquid drops (4). The drop acceleration is known once the gas density ρ and velocity U is stated.

$$\boxed{\frac{dV}{d\theta} = -\frac{3}{8} C_D \frac{\rho}{\rho_L} \frac{(U-V)^2}{r}} \qquad (9)$$

and is taken to have the same sign as (U - V). V is the drop velocity in ft/sec and C_D, the drag coefficient is given by:

$$C_D = \frac{27}{Re^{.84}} \qquad (10)$$

Drop breakup was considered necessary since high pressures, above the critical temperature of the fluid, would be used. Liquid temperatures could not, physically, go to the critical without reduction of surface tension, σ_L, to the point where droplet stability is impaired. Therefore, provision was made for the droplet to be replaced by an arbitrary number of smaller drops of equal mass whenever an arbitrary Weber number was exceeded.

$$We = \frac{2r(U-V)^2\rho}{\sigma_L} \qquad (11)$$

This number is a ratio of the distorting force to the restoring force. This is intended as a zero order approximation to qualitatively determine what effects may occur.

THE HYDRODYNAMIC MODEL

The thermodynamic properties of the combusted fuel and oxidizer were obtained from the Second Law restriction that the Free Energy must be a minimum at a given value of pressure and temperature for an equilibrium condition. The reaction equations used are:

$$CO_2 - CO \longrightarrow O \qquad \tfrac{1}{2}CO_2 + \tfrac{1}{2}H_2O - \tfrac{1}{2}CO \longrightarrow OH$$

$$2CO_2 - 2CO \longrightarrow O_2 \qquad CO + H_2O - CO_2 \longrightarrow H_2$$

$$\tfrac{1}{2}CO + \tfrac{1}{2}H_2O - \tfrac{1}{2}CO_2 \longrightarrow H$$

These equations are written in the form of

$$\Delta G_j = \sum_i \mu_i \nu_{ij} \qquad (A)$$

where

$$\mu_i = \left(\frac{\partial G}{\partial n_i}\right)_{T,P,n_j}$$

and ν_{ij} is the coefficient of the i th component of the j th reaction. n_i is the number of moles of specie i. The change in n_i species are limited by the restraint

$$dn_i = \sum_j \nu_{ij}\, d\xi_j \qquad (B)$$

Here ξ is the extent of the reaction.

Also at a fixed T and p

$$dG = \sum_i \mu_i\, dn_i \qquad (C)$$

A parameter λ is introduced such that

$$d\xi_j = -\Delta G_j\, d\lambda$$

Then with (A), (B) and (C) we obtain

$$dG = -\left\{\sum_j (\Delta G_j)^2\right\} d\lambda = \sum_i \mu_i\, dn_i \qquad (D)$$

If $d\lambda > 0$, then a thermodynamically possible change in G can occur, i.e., G decreases. From this form, the sum of the squares of ΔG may be computed and the computation terminated when $\sum_j (\Delta G_j)^2 \leq \delta$, δ is determined from the accuracy of the free energy data. A more detailed discussion is given in (7).

Once the minimum value of free energy is determined, then the species n_i are known and, with a knowledge of the specific heat data, the enthalpy and molecular weight of the mixture may be determined. These two values are used in the energy equation (10) and the equation of state (12).

The relations for the steady state equations may be obtained from the nonsteady equations (5). These equations relating the gas pressure P, density ρ, temperature T, and velocity U are the equation of state:

$$P = \left(\frac{R_o}{M}\right) \rho T \qquad (12)$$

$\left(\frac{R_o}{M}\right)$ is the gas constant.

The continuity equation:

$$\frac{\partial \rho A}{\partial \theta} + \frac{\partial (\rho U A)}{\partial x} = \dot{W} \qquad (13)$$

A is the chamber cross sectional area, ft^2

$\dot{W}$ is the mass added per unit length per unit time.

The momentum equation:

$$\frac{\partial U}{\partial \theta} + U \frac{\partial U}{\partial x} = -\frac{1}{\rho} \frac{\partial P}{\partial x} + f \qquad (14)$$

f is the force between the liquid drops and gas, $\frac{\text{ft-lbf}}{\text{lbm}}$

The energy equation following a gas particle is:

$$\frac{\partial h}{\partial \theta} + U\frac{\partial h}{\partial x} = \dot{q} + \frac{1}{\rho}\frac{\partial P}{\partial \theta} + \frac{U}{\rho}\frac{\partial P}{\partial x} \tag{15}$$

This equation can be reduced to a relation between thermodynamic states once the relation between enthalpy (h) and temperature is known.

For the steady state all time derivatives may be dropped from (13) and (14) so that:

$$d(\rho UA) = \dot{W}\,dx$$
$$U\,dU = -\frac{1}{\rho}\,dP + f\,dx$$

The integrated continuity equation becomes

$$\boxed{(\rho UA)_x = \int_0^x \dot{W}\,dx = \phi_x} \tag{16}$$

The integrated momentum equation becomes

$$\boxed{P_{x+\Delta x} = P_x + {}_x\rho_{x+\Delta x}\left[\int_x^{x+\Delta x} f\,dx + \frac{U_x^2 - U_{x+\Delta x}^2}{2}\right]} \tag{17}$$

The energy equation for a control volume is:

$$\boxed{\begin{aligned}&\phi_x\left(C_p T_x + \frac{U_x^2}{2}\right) - \phi_{x+\Delta x}\left(C_p T_{x+\Delta x} + \frac{U_{x+\Delta x}^2}{2}\right) = \\ &= (\phi_{x+\Delta x} - \phi_x)\left(C_p T_f + \frac{V^2}{2}\right) + q_v\end{aligned}} \tag{18}$$

Here q_v is obtained from equation (2).

V is the drop velocity and T_f is the flame temperature.

Equations (12), (16), (17), and (18) combined with (3), (8) and (9), written in finite difference form, from the set of equations to be solved.

The Strategy of Computation

The calculation was divided into two main parts. In the first part a single droplet is followed as it moves, evaporates, and breaks up, in a prescribed environment of gas pressure, temperature, and velocity.

Equations (3), (8), and (9) are simultaneous ordinary differential equations in the variables T_L, r, and v, and can be solved if initial conditions plus values of T, p, and U as all points are known. This is repeated for each drop size present, and the results weighted to give the total evaporation.

In the second part, the hydrodynamic equations are solved for a specified evaporation profile taken from the results of part one. Equations (12), (16), (17) and (18) are solved simultaneously, since $\phi(x)$, $q_v(x)$, $f(x)$ are known from the evaporation calculation. The boundary conditions for the gas dynamic equations are given as:

$$\text{at } x = x_o \qquad p = p_o,\ T = T_f,\ U = 0$$

$$\text{at } x = L \qquad U_L = \sqrt{\delta RT_L}$$

100 basic increments were subdivided into a number of sub-steps which were determined by the slope of the evaporation curve. With 10 sub-steps, satisfactory results were usually obtained. Normally, 1000 increments were used, unless the liquid temperature changed by more than $50^{\circ}F$ in an increment. In this case, the increment size was reduced by

a factor of 10 for that sub-step. If the liquid temperature change was still too large, then then the sub-step was reduced by 10^2, etc. This insured slowly changing integrands and provided satisfactory convergence for all cases tried. Physical properties, which were needed in computation of equations (1) thru (11) were provided by a series of subroutines, using a variety of equations, as well as tables with interpolations. Change of any basic equations would require altering the evaporation subroutine. Change in physical properties, other than input quantities, can be made by replacing the appropriate subroutine.

In the evaporation subroutine, droplet breakup takes place according to the Weber number criterion, equation (11).

After computing evaporation, the main program weights the results to compute total evaporation at each increment, which is part of the input information to the fluid dynamics subroutine.

In equations (12), (16), (17) and (18) form the heart of the fluid dynamic subroutine. The program uses information given to it by the evaporation subroutine to produce a matrix (3 x 100) of gas pressure, temperature, and velocity. That is, the combustion chamber and nozzle are divided into 100 sections (1, 2, 3,.....n, n + 1.....100). A separate calculation is carried out in each section, that is, going from (n) to (n + 1).

The area which is available to gas flow A_n, A_{n+1}, is calculated by a subroutine program and also the total mass that is present at any section ϕ_n, ϕ_{n+1} is obtained by a function program. The subroutine checks the ratio of the terms, i.e., ϕ_{n+1}/ϕ_n and if a prescribed limit is exceeded, the step size

$$\chi_{n+1} - \chi_n = \quad _n \triangle \chi_{n+1}$$

becomes

$$\Delta x' = \frac{n}{N} \Delta x_{n+1}$$

where N may be any convenient number such that $\frac{\phi_{n+1}}{\phi_n} \longrightarrow 1$. Here the primes denote the new coordinate. The computational procedure is carried out N times, then the ratio $\frac{\phi_{n+2}}{\phi_{n+1}}$ is checked, and so on. The method of solution consists of assuming a T_{n+1} and solving for U_{n+1} in equation (16). Then one may solve for p_{n+1} knowing the U_{n+1} from equation (17) and p_n from (12). T_{n+1} may be solved for in equation (18) and if

$$\left| T'_{n+1} - T_{n+1} \right| < \epsilon \quad , \epsilon > 0$$

then we say that the system of difference equations (12), (16), (17), and (18) are satisfied. We now proceed in the space calculations by assuming T_{n+2} and continue in a similar manner. The superscripts denote iteration number. Transfer after completion of 100 steps is to the main program, which controls the drop and gas calculation.

DESCRIPTION OF EXPERIMENTAL APPARATUS

The first series of tests were conducted with liquid oxygen and JP-5A in a two inch diameter chamber, employing a showerhead type injector and a simple converging-diverging nozzle, (Fig.1). The only variable in this first series of tests was the chamber length, i.e., using the same injector-nozzle configuration, and the same propellant flow rates, the chamber length was to be varied from 8 to 24 inches. Therefore, the chamber may be composed of one or more sections depending upon the total length desired. The three basic components, (injector,

chamber, and nozzle), are held together by means of a mechanical clamping arrangement. All components are uncooled, and are fabricated from commercial brass, with the exception of the nozzle. This is composed of a graphite liner in a brass collar, and is also uncooled. A complete description of the feed system, control system, and rocket motor can be found in (8).

The design of the nozzle for the steady state program was influenced by the future objectives of the Laboratory. Among these objectives was an investigation of the non linear aspects of combustion instability. In the theoretical analysis of combustion instability, the effect of the Mach number of the gases is highly significant, as indicated in (3). Briefly stated, if $(1-M^2)$ is approximately unity, i.e., if M is approximately 0 2 or less, the mathematical analysis can be greatly simplified by means of linearizing assumptions. However, the actual problem is non linear, and in practice the Mach numbers at the nozzle entrance are well above the "linear" value of 0.2. Since the entire steady state program was being conducted as a preliminary step to a non-steady non linear analysis of combustion instability, the nozzle contraction ratio was designed for a nozzle entrance Mach number of .45, based upon isentropic flow and constant isentropic exponent.

The verification of the nozzle entrance Mach number required a measurement of the total pressure at that point. This entails designing a probe that can exist in an extremely high temperature, oxidizing atmosphere. A water-film cooled graphite probe was developed and employed successfully, (Fig.2). The cooling water is sprayed through the probe body into the gas stream at a pressure slightly in excess of the gas pressure. Thus, a film type cooling is obtained. The mass flow of water into the chamber amounts to only 1 % of the propellant flow.

The instrumentation necessary for the measurement of static pressure gradients in a rocket motor was selected after a consideration of several factors: namely; proximity of measurements, expected pressure gradient, accuracy, and cost. Assuming that the pressure was to be measured at eight longitudinal locations, the obvious solution would be to install eight transducers down the length of the chamber. However, each of the considerations above eliminated this technique. Tests conducted on the shorter length chambers would require a pressure measurement at one inch intervals. The physical size of the diaphragm on a water cooled transducer varies from 1/2 to 1 inch depending on the manufacturer. Therefore, each transducer would actually measure an average pressure over an interval comparable to the center to center distance between pressure taps. In addition, it was expected that the gradient at certain sections of the motor would be as small as 1 psi in 200 psi between adjacent taps. Using a 500 psi full range transducer, a drift of .1 % of full scale in opposite directions by two adjacent transducers would yield zero pressure gradient. Rather than develop a method of compensating for the different drift characteristics of adjacent transducers and associated electronics, it appeared more feasible to develop a technique that employed a single transducer to measure the pressure gradient. In addition, if such a system could be developed the dollar savings to the experimental program would be significant. Rather than employ eight water cooled transducers it would be possible to use a single transducer. It will subsequently be shown that the transducer need not be cooled, resulting in an additional savings. All of the above-mentioned factors lead to the development of a pressure scanner (Fig.3).

The scanner permits a single transducer to travel from pressure tap to pressure tap and consecutively record the pressure at eight different locations in the chamber. The pressure scanner consists of three piston and cylinder units. Units A and B each contain facilities for measuring the pressure at eight locations, while unit C is a hydraulic driver. The taps located in the rocket motor are extended to the bulkhead of either unit A or B and then to compartments formed by the inner cylinder or piston, "O" rings, and the outer travelling cylinder which houses a transducer. The reciprocating motion of the outer cylinders, (which enables the transducer to consecutively measure the pressure at adjacent taps in the rocket motor) is governed by a double acting hydraulic piston and cylinder; unit C. Provisions have been made for varying the speed and length of stroke of the unit. In addition, a method of continuously recording the exact location of the transducer housing has been developed. This consists of measuring the voltage drop between a moving electrical contact mounted on the transducer housing and a flat copper bar mounted alongside the scanner cylinder. The copper bar is actually an eight stepped voltage divider. The length of each step is equal to the length of the compartments in the scanner cylinder. The distance between steps or sections is equal to the thickness of the "O" rings separating the compartments. Each of the copper bar sections is a a different predetermined voltage. Therefore, by simultaneously recording the output of the transducer and the voltage drop to the moving electrical contact, it is possible to match the pressure magnitude with the location at which it was measured.

The output of the transducers is recorded on a recording oscillograph. To record the absolute pressure at each port would result in reduced resolution. Therefore, only the pressure difference about a fixed point is recorded.

Thus 40 psi rather than 200 psi is full-scale deflection on the recorder. The above technique is accomplished by several methods depending upon the type of transducer employed in the scanner. Using a piezoelectric, crystal transducer, the crystal is grounded until the starting transient has been completed. The pressure on the transducer diaphragm at the instant that the ground connection is broken and all subsequent pressures to be measured is recorded. To determine the absolute pressure at each port, from the records of the gradients, requires a measurement of the absolute pressure at one point in the chamber.

Several objections may arise as to the accuracy and applicability of the above described system for the measurement of pressure gradients in a rocket motor. It is obvious that the pressure at each chamber tap is not measured simultaneously, but rather there is a time lag between the measurement at successive ports. However, the speed of the scanner can be adjusted so that a complete traverse of the chamber can be made in one second. Since a normal test firing lasts six seconds after steady state conditions have been reached, six complete traverses of the motor can be obtained in one run. Examination of the data indicates that one traverse is identical to the next, both as to gradient and absolute pressure at each port. Thus, it is concluded that once the maximum chamber pressure has been reached, the motor operation is steady in time unless an instability arises.

In spite of the previous remarks regarding the steadiness of operation and the reproducibility of gradients on a recording trace during a test run, the pressure at each chamber location is not invariant. Under the smoothest conditions there is still a good deal of combustion noise present. In addition, as pointed out in (3) and (4), there exists an instability regime for any particular oxidizer- fuel ratio of a given set of propellants. During the course of the tests, "rough" or "unstable" operation was encountered

on several occasions, particularly with the shorter chambers, ranging in length from eight to twelve inches. Further discussion of the occurence of pressure oscillations in excess of combustion noise is presented in the discussion of experimental results. Despite the above comments, it is still possible to determine the steady state pressure gradients, where steady state is defined as the average or D.C. level of the transducer output.

EXPERIMENTAL RESULTS - COMPARISON WITH THEORY

Steady state pressure gradients were measured in a two inch diameter variable length rocket motor. Initially, static pressure was measured at seven longitudinal locations and total pressure was measured approximately one inch from the nozzle entrance. After it was determined that the nozzle entrance Mach number was greater than 0.4 the total pressure measurements were abandoned. Subsequently, it became possible to measure the static pressure gradient at eight longitudinal locations.

The first series of tests were conducted on a 17 inch chamber length. The results are plotted in Figure (4). Results indicate the prescence of a steep pressure gradient between four and ten inches from the injector face. The data indicates that a 29 psi gradient was measured between $1\frac{1}{4}$ and $14\frac{3}{8}$ inches from the injector face. This amounts to 17 % of the pressure measured at the $1\frac{1}{4}$ inch tap. In the region between four and ten inches from the injector, (35 % of the chamber length), a gradient of 21 psi was measured. This is equal to 72 % of the measured total gradient, or a somewhat smaller percentage of the gradient obtained by extrapolating to the injector face and nozzle entrance. According to the analysis set forth in (1), the major portion of combustion takes place in this steep pressure gradient region. The gradient in the remaining portion of the chamber,

(10 - 17 inches), is flat; 7 psi in 7 inches. It is felt that this portion of the pressure drop is due to heat transfer and low friction. The ratio of static to total pressure is 0.915 at the 14 $\frac{3}{8}$ inch tap. This corresponds to a Mach number of 0.41 for a gas whose isentropic exponent is 1.11. The value of 1.16 was determined by the analysis set forth in (1). The oxidizer fuel ratio for this, and all subsequent tests discussed in this report is 2.76 $\pm$ 5%. The total propellant flow is 2.47 lbm/sec $\pm$ 5%. The O/F equivalence ratio is 0.793. The percentage deviation stated above does not account for the experimental error in a single test, but is due to a variation in measured flow from one test to another.

The theory predicted that the main evaporation and combustion of the drops occured within a fractional section of the chamber length. Here the fluid dynamic flow field increased the evaporation rate which in turn increased the velocity field and hence the pressure gradient.

Typical results of the integration of equations (3), (8), (9), (12), (16), (17) and (18) are shown in Fig.4. Curve A is the solution for p(x) when the boundary condition for temperature at the injector is equal to the flame temperature (5877°R). Curve B is the solution for p(x) when the gas temperature at the injector face is 5500°R. Curve B is intended to show the effect of heat transfer or combustion efficiency on the pressure drop. Curve B allows a greater mass flow through the nozzle due to lower chamber temperatures. ϕ_{max} = 2.36 is the experimentally measured flow rate.

In order to determine the effect of chamber length on the position of the steep portion of the gradient, and hence the combustion process, the chamber was reduced to 8 $\frac{3}{8}$ inches with subsequent tests to be run with chamber length increments of two to three inches. The gradients obtained in an 8 $\frac{3}{8}$ inch chamber and a 10 $\frac{3}{8}$ inch chamber are presented in Figure 5. Both curves indicate a continuously increasing gradient over a region that

extends approximately one inch from the injector face to one inch from the nozzle entrance. It was stated previously that the gradient in the 17 inch chamber, Figure(4), started to decrease ten inches from the injector face. As a result of the increasing gradient at the nozzle entrance, it is concluded that evaporation and combustion of the fuel is not completed in the shorter chambers. This is in agreement with the predictions of the theoretical analysis which is also shown in Figure (5) and Figure (8). The Mach number at a point one inch from the nozzle entrance of the $8\frac{3}{8}$ inch chamber was 0.23, as compared with 0.41 for the 17 inch chamber. The low Mach number is attributed to the low gas generation rate in the shorter chambers. In addition, the velocity increment of the gases through the last inch of the chamber is much greater for the shorter lengths than for the 17 inch motor. This is due to the fact that evaporation and combustion is still present in the short chambers, while it virtually has been completed in the longer chambers. Results from additional tests with the $8\frac{3}{8}$ inch motor indicate that is is possible to increase the Mach number by increasing the O/F ratio. Since the main body of tests were run with fuel rich mixtures, an increase in the O/F ratio brings it closer to stoichiometric proportions, causing a more complete combustion process in the chamber, and a higher Mach number at a point one inch before the nozzle.

The experimental results obtained with a $12\frac{1}{4}$, $15\frac{1}{2}$, and $19\frac{1}{4}$ inch chamber are reproduced in Figure (6). All three tests indicate a decreasing gradient, or point of inflection, approximately ten inches from the injector face. The gradient in the region of the injector face appears to be steeper in the case of the $12\frac{1}{4}$ inch chamber, than in the longer lengths. This would indicate a rapid breakup of the injected spray, and hence evaporation

and combustion closer to the injector face.

The above phenomenon, (steep pressure gradients at the injector face) is also present, though to a somewhat lesser extent, in the $8\frac{3}{8}$ and $10\frac{3}{8}$ inch chambers. The steeper gradients, indicative of jet-breakup and droplet evaporation, is attributed to "rough" or "unstable" operation. Due to the low frequency response of the recording oscillograph it is not possible to quantitatively describe the pressure oscillations. However, based upon the relative amplitude of the pressure oscillations and the frequency of chamber and nozzle burnout, the $12\frac{1}{4}$ inch chamber would be the most unstable configuration. The oscillations in the shorter chambers were of a lesser degree, whereas the longer lengths exhibited only normal combustion noise. It is felt that the increased pressure oscillations in the shorter chambers causes a more rapid breakup of the injected spray, resulting in a shift of the combustion zone towards the injector face. Previous work done at the Propulsion Research Laboratory, (11) discusses in detail, the effect of chamber length and pressure oscillations on liquid jet breakup.

It might be mentioned at this time that the steady state analytical work did not include the jet-breakup distance. It appears to be a critical factor for the initiation point of the evaporation computation. A fixed value of 2 inches was used in all computations for qualitative purposes. A more complete analysis would incorporate a mechanism for jet breakup and drop formation. It would appear from the results obtained under stable conditions, that this 2 inch distance is of the right order of magnitude. Lawhead of Rocketdyne in private communication has also indicated a 2 inch region with similar injector configurations. He obtained this result with streak photography.

A question may arise as to a reason for the variation of absolute pressure at the injector face for the test results presented. Actually, the variation is only 3 per cent, and is equivalent to the error associated with the bourdon tube pressure gauge used to measure the reference absolute pressure at a point in the chamber. It was previously stated that the reference pressure was used only to convert the pressure gradient recordings into absolute pressure distributions. The significance of the variation is very slight. It should be stressed that the main function of the experimental program was to determine the pressure gradient for a given set of injector boundary conditions. A variation of 1 or 2 psi in the absolute pressure would have little or no effect on the gradient for a given set of injection parameters.

Figure 7 shows the effect of initial drop radius on the position of the pressure gradient in the 15.5 inch chamber. The three drop model uses a Rosin-Rammler distribution (12) to describe the spray distribution. The small drops, which make up 28 % of the spray (represented by the 26μ drop), evaporate and combust quickly. The pressure gradient is thus initially steep and results in accelerating the evaporation process of the larger drops. The 80 micron drop is, thus, completely evaporated within the chamber. On the other hand, the 100 micron model evaporates very much more slowly due to the absence of this interaction, and so a 15.5 inch chamber is insufficient for proper combustion.

Figure 9 shows the gas temperature and velocity as a function of position in the 15.5 inch chamber. Figure 10 shows the results of the solution of the differential equations of the liquid subsystems for the 15.5 inch chamber. The liquid temperature rises rapidly but then remains practically constant throughout evaporation. r/r_o initially increases due to expansion and then

decreases due to evaporation. In this case $r_o = .19 \times 10^{-3}$ Ft, $V_c = 122$ Ft/sec and $T_o = 600^\circ R$.

CONCLUSIONS

The picture is, then, one of slowly evaporating drops flowing down a field of gradually increasing velocity until a co-operative effect between the drops and flow field causes an acceleration of evaporation. In certain cases it has been found that if the velocity gradients are really severe, shattering of the droplets occur. This happened in the nozzle of the 8 inch chamber.

When the Weber number is given a value of 100, droplet shattering (Fig.8) occurs in the chamber (dashed curve) and drastically changes the picture of evaporation. Just as in the case of drops in a spray with continuous evaporation a similar effect occurs with breakup. When the drops start breaking up evaporation increases very quickly causing a pressure drop with a corresponding increase in the gas velocity. The resulting velocity gradient then increases the breakup, etc. The basic difference between continuous evaporation model, and the breakup model is the thickness of the energy release zone ($\dot{W}(x) = \frac{J\Phi}{Jx}$).

For a given set of injection parameters under stable operating conditions, the results indicate that the steepest portion of the gradient, which corresponds to evaporation of the major portion of the fuel, is always found in a fixed region of the chamber, independent of the absolute length of the motor. For the tests discussed in this report, the steepest portion of the gradient was located between four and ten inches from the injector face. Chambers shorter than ten inches exhibited combustion in the nozzle. It was also found that "rough" or "unstable" operation shifted the gradient. Increasing pressure oscillations caused a shift of the steep portion of the gradient

towards the injector face.

In conclusion, it appears that evaporation is a proper rate controlling mechanism for the cases investigated. By proper shaping of the combustion chamber the evaporation schedule may be extended over the entire chamber length, i.e., a pear shape may distribute the energy release pattern (ϕ) evenly over the entire chamber. An inverse effect may be created by introducing constrictions in the combustion chamber to localize combustion by shattering the droplets in a high velocity gradient field.

Finally, it must be observed that the intent of the experimental program was to determine steady state pressure gradients for verification of the theoretical analysis and any conclusions based upon the experimental program alone requires further substantiation. The analytical work will be extended to a nonlinear nonsteady instability analysis using the results of the present investigation.

ACKNOWLEDGEMENTS

The authors wish to express their gratitude to Dr. Robert Corry for his valuable suggestions and to Mr. William Peschke and Mr. Imants Reba for their participation in the experimental program. Much appreciation is also given to Mr. A. Burstein for the drawing of the figures.

REFERENCES

1. Ranz, W.E. and Marshall, W.R. Jr., "Evaporation from drops" Part I, Chemical Engineering Progress, Vol. 48 pp 141-146 (1952)

2. Bird, R.B., "Theory of Diffusion", Advances in Chemical Engineering, Academic Press, New York 1956.

3. El Wakil, M.M., Uyehara, O.A., and Myers, P.S., "A Theoretical Investigation of the Heating-up Period of Injected Fuel Droplets Vaporizing in Air", National Aeronautics and Space Administration T.N. 2368 (1954)

4. Ingebo, R.D., "Vaporization Rates and Heat Transfer Coefficients for Pure Liquid Drops", National Aeronautics and Space Administration T.N. 2368 (1951)

5. Torda, T.P., Burstein, S.Z., "Non linear Theory of Combustion Instability-Liquid Propellant Rocket Motors". Propulsion Research Laboratory PRL-TM-58-1 (December 1958), ASTIA No.209-491, AFOSR Doc. No. TN 59-60

6. Priem. R.J., "Propellant Vaporization as a Criterion for Rocket Engine Design; Calculations of Chamber Lengths to Vaporize a Single n-Heptane Drop. National Aeronautics and Space Administration TN 3985 (1957)

7. Naphtali, L.M. "Complex Chemical Equilibria by Minimizing Free Energy" AFOSR Doc. No. TN 60-228, Project No. 9751.

8. Corry, R. and Peschke, W., "The Propulsion Research Laboratory of the Polytechnic Institute of Brooklyn", A Symposium on Jet Propulsion, Polytechnic Institute of Brooklyn, Feb. 1961.

9. Crocco, L., Grey, J., and Harrje, D., "Theory of Liquid Propellant Rocket Combustion Instability and its Experimental Verification", Journal of the American Rocket Society, Vol. 30, No. 2, 1960, p.159.

10. Zucrow, M.J., and Osborn, J.R., "An Experimental Study of High-Frequency Combustion Pressure Oscillations", Jet Propulsion Vol.28, No.10, Oct. 1958, p.654.

11. Reba, I., and Brosilow, C., "The Response of Liquid Jets to Large Amplitude Sonic Oscillations", WADC Technical Report 59-720 Part III.

12. Burstein, S.Z., Naphtali, L.M., "A Spray Combustion Model with Droplet Breakup", Kinetics, Equilibria and Performance of High Temperature Systems Proceedings of the First Conference, by Butterworth and Co.

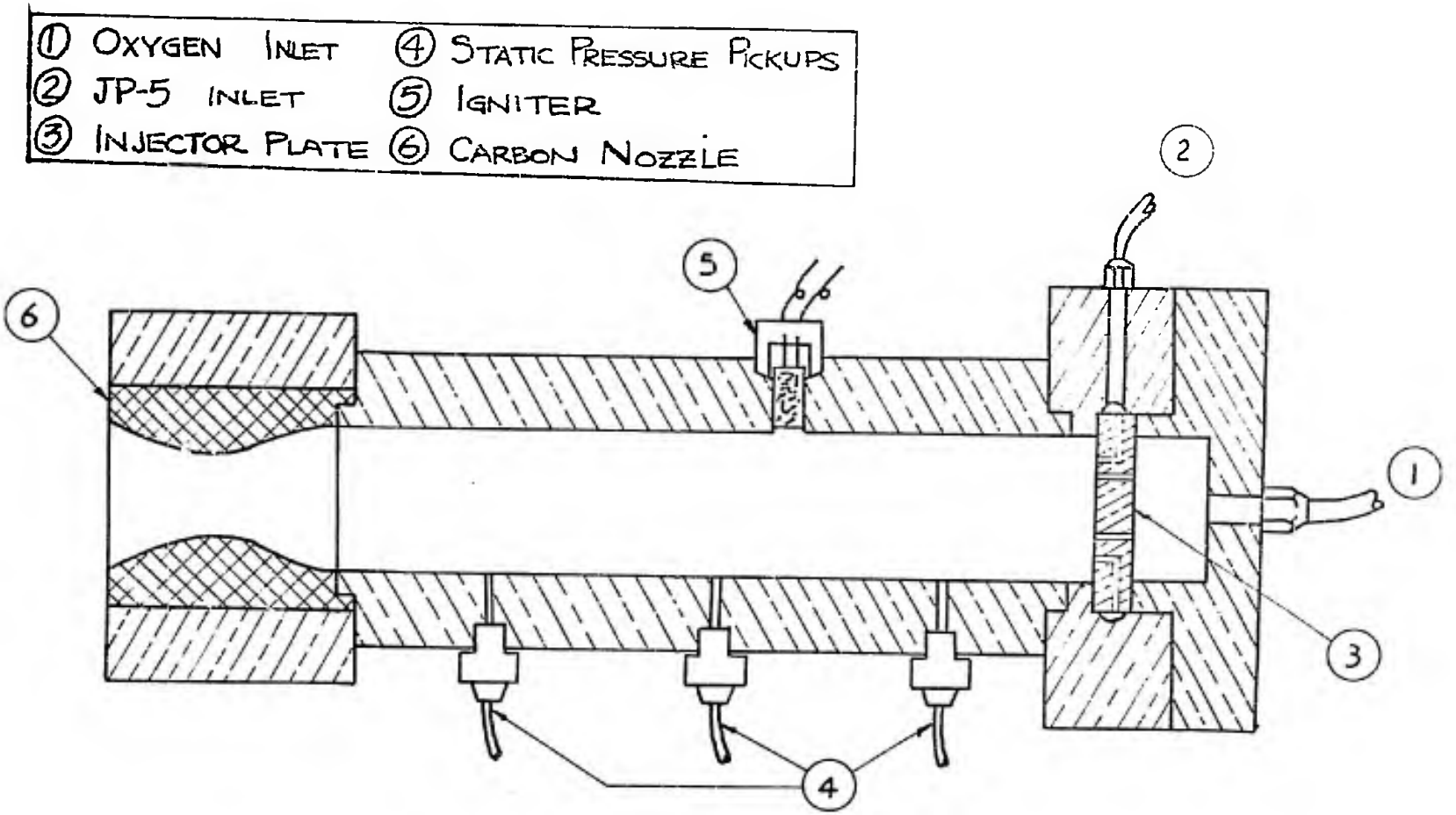

Rocket Engine Section

Figure 1

WATER COOLED CARBON PROBE

FIGURE 2

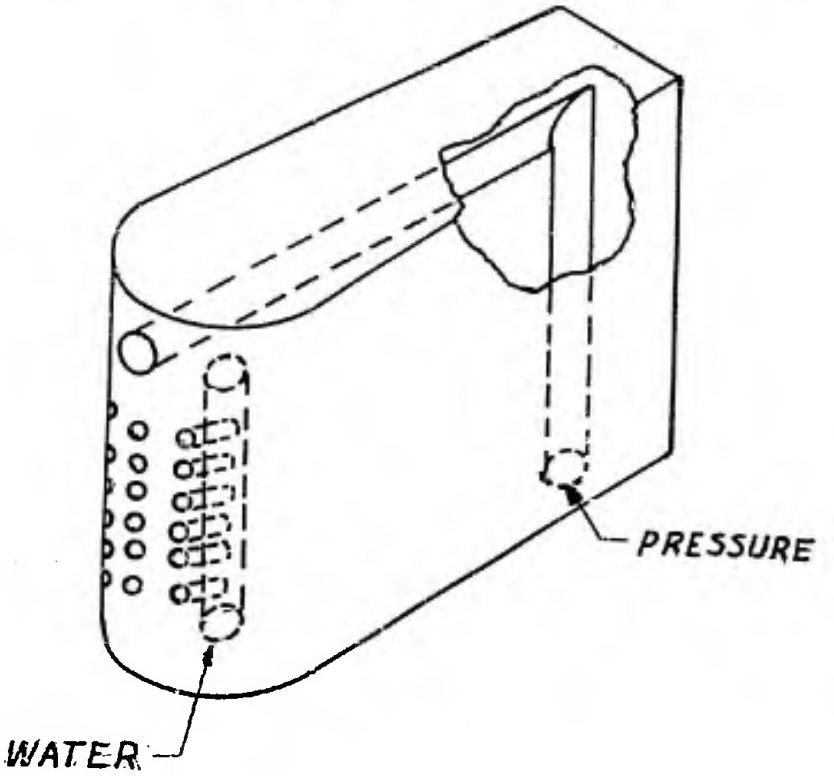

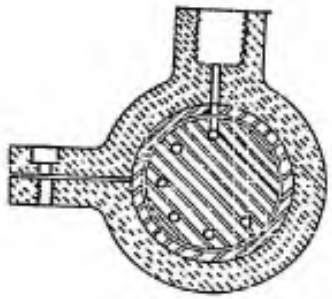

SECTION B
DOUBLE SIZE

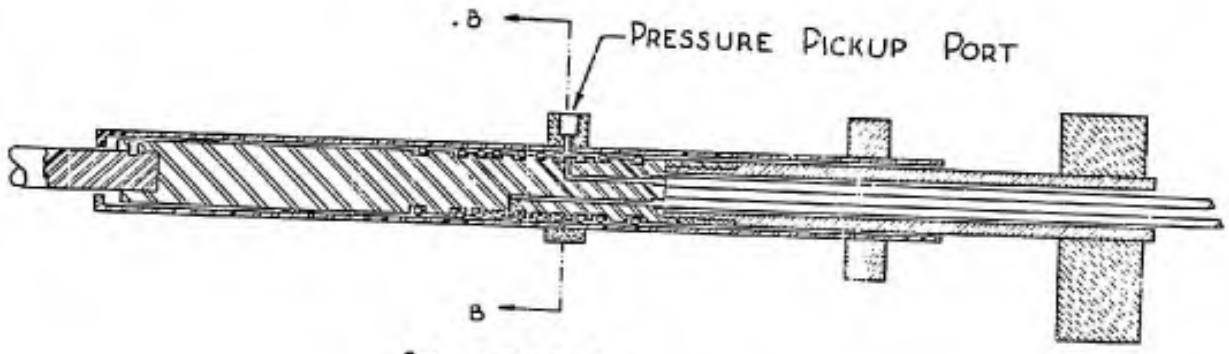

SECTION A

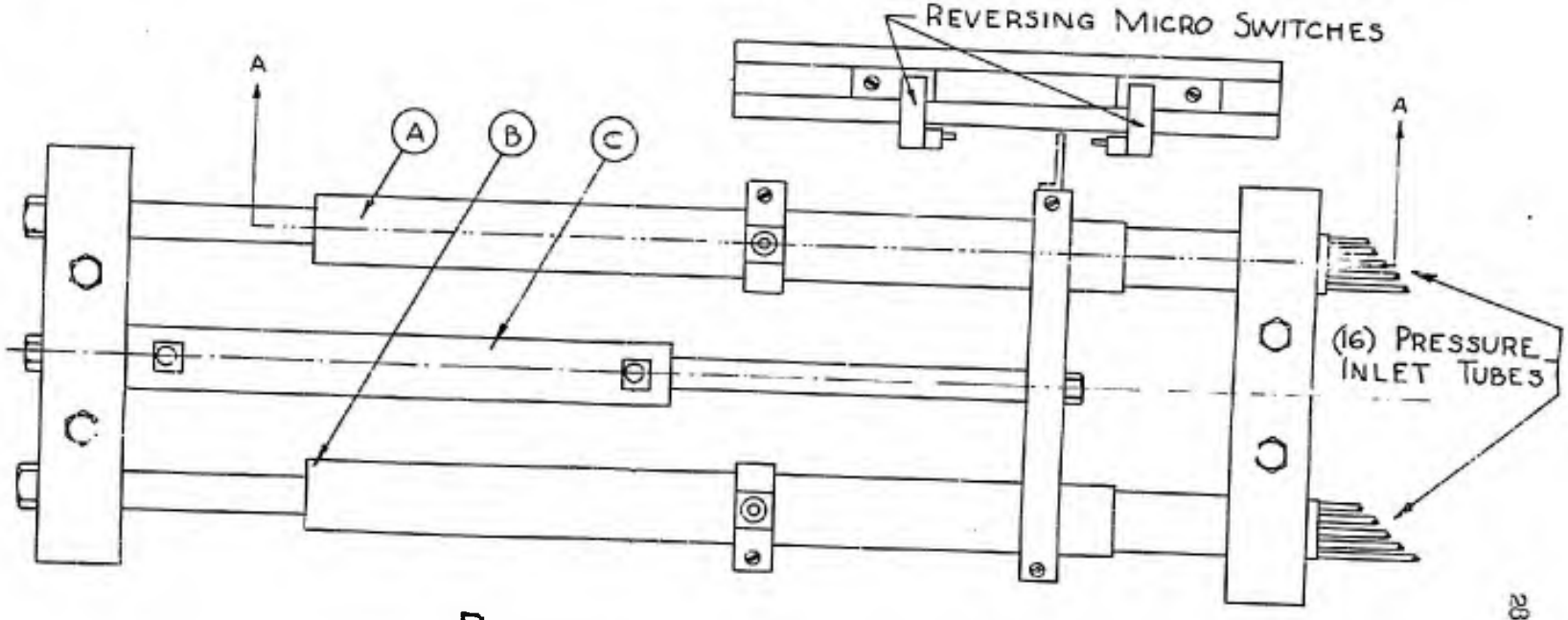

PRESSURE SCANNER
FIGURE 3

SCALE: 3 IN. = 1 FT.

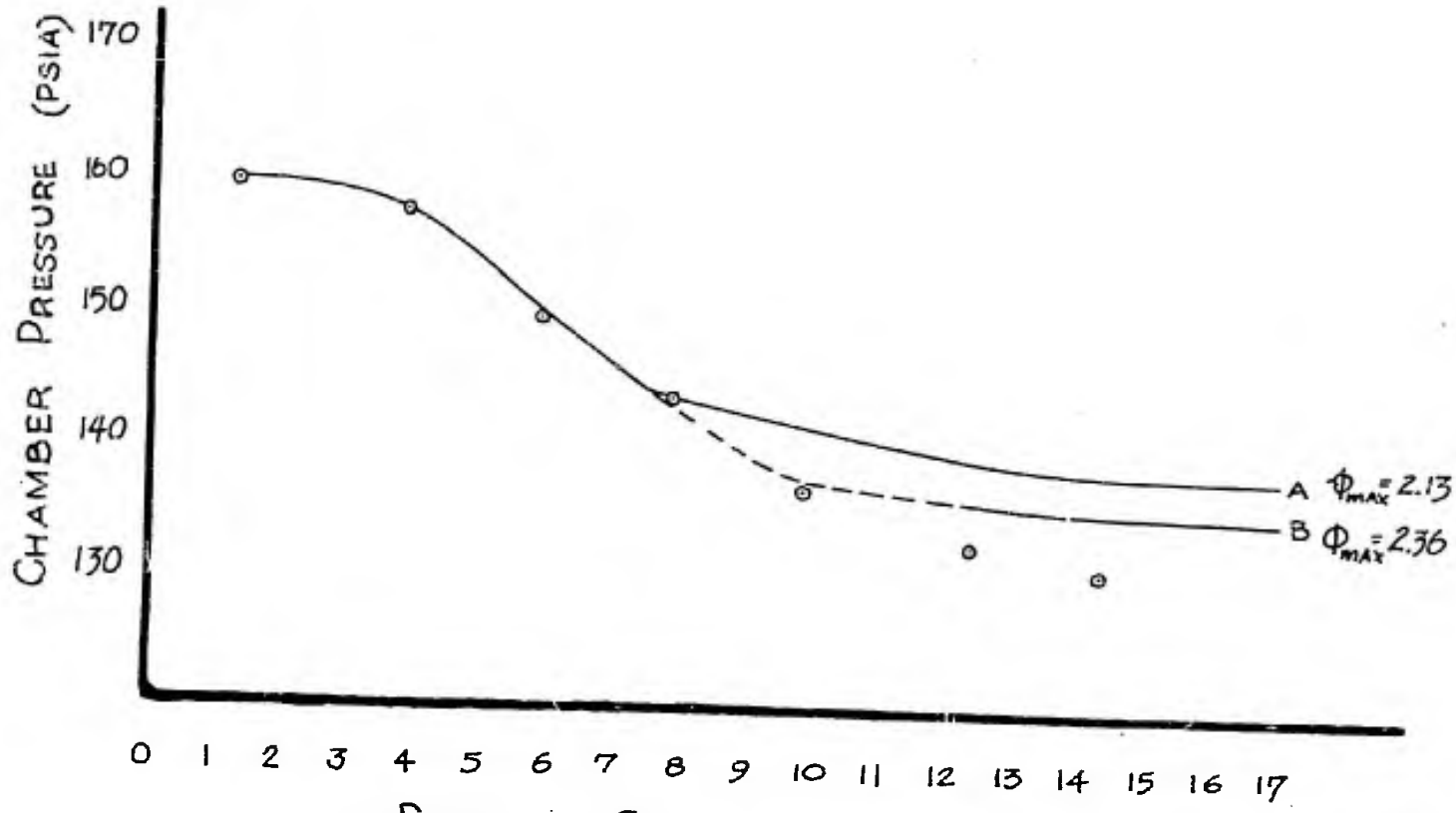
CHAMBER PRESSURE (PSIA)
170
160
150
140
130
A $\Phi_{max} = 2.13$
B $\Phi_{max} = 2.36$
0 1 2 3 4 5 6 7 8 9 10 11 12 13 14 15 16 17
DISTANCE FROM INJECTOR (INCHES)

FIGURE 4

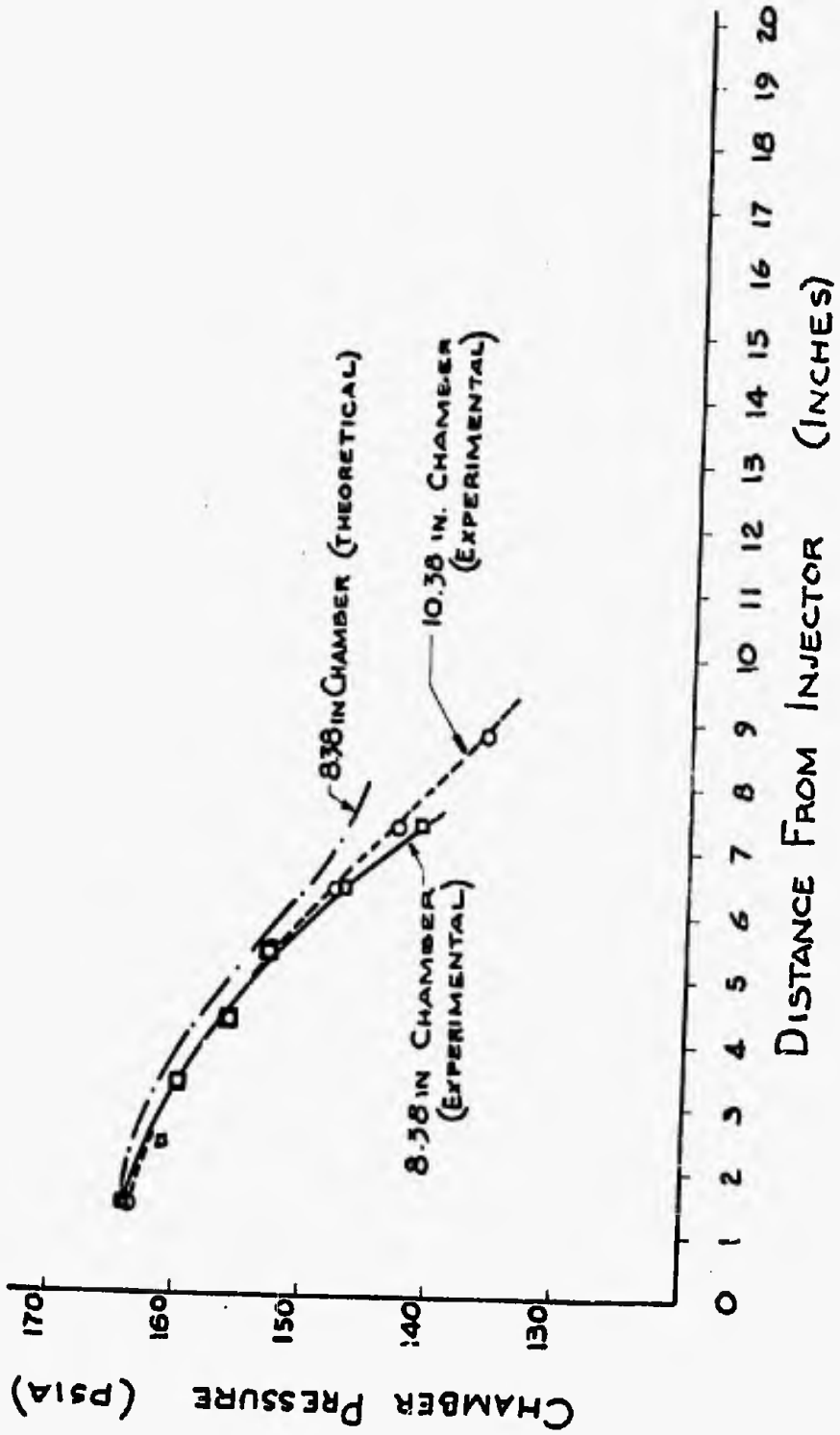
CHAMBER PRESSURE (PSIA)
170
160
150
140
130
0 1 2 3 4 5 6 7 8 9 10 11 12 13 14 15 16 17 18 19 20
DISTANCE FROM INJECTOR (INCHES)
8.38 IN CHAMBER (EXPERIMENTAL)
10.38 IN. CHAMBER (EXPERIMENTAL)
8.38 IN CHAMBER (THEORETICAL)

FIGURE 5

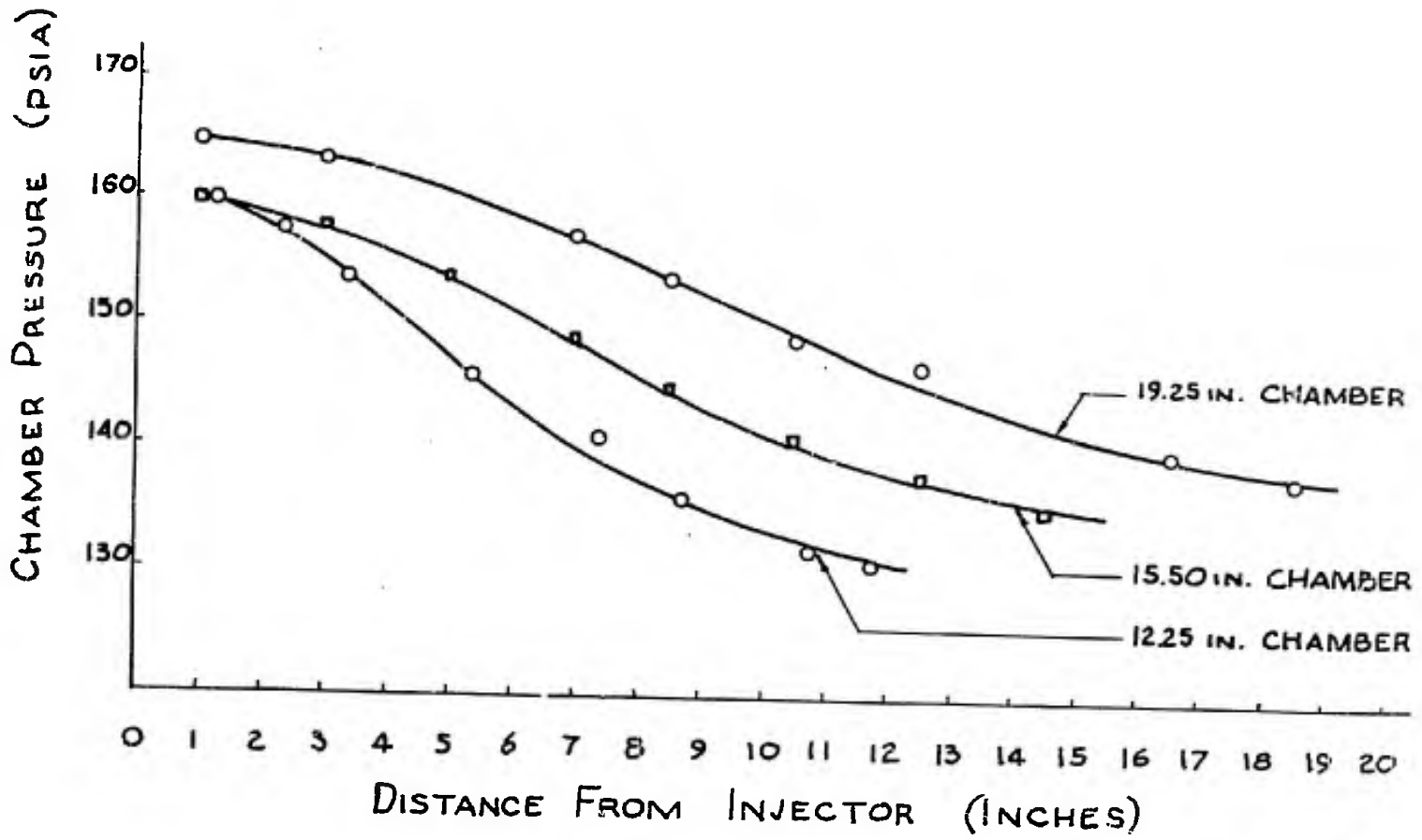
CHAMBER PRESSURE (PSIA)
170
160
150
140
130
19.25 IN. CHAMBER
15.50 IN. CHAMBER
12.25 IN. CHAMBER
0 1 2 3 4 5 6 7 8 9 10 11 12 13 14 15 16 17 18 19 20
DISTANCE FROM INJECTOR (INCHES)

FIGURE 6

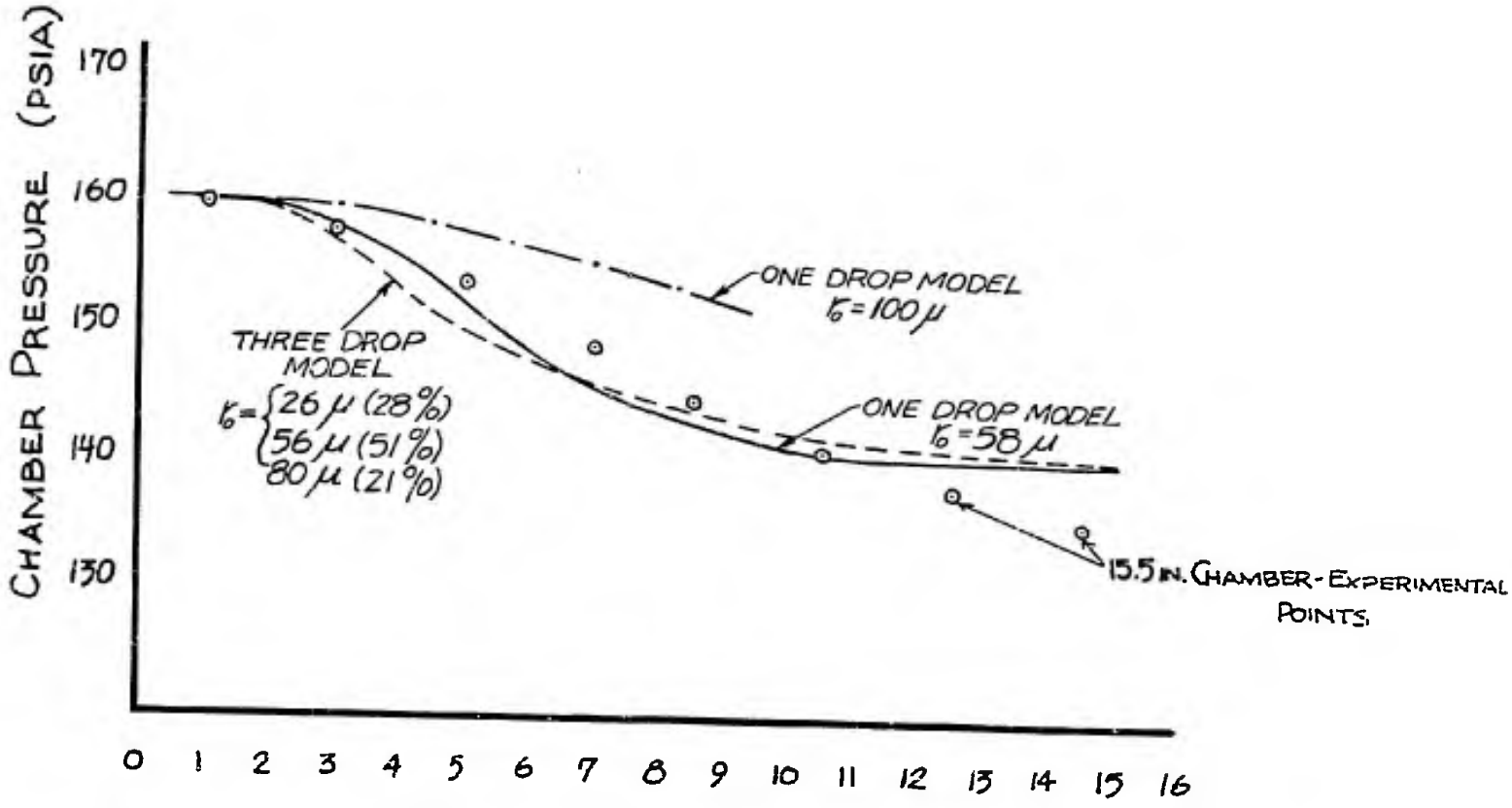
CHAMBER PRESSURE (PSIA)
170
160
150
140
130
ONE DROP MODEL
r₀ = 100 μ
THREE DROP MODEL
r₀ = 26 μ (28%)
56 μ (51%)
80 μ (21%)
ONE DROP MODEL
r₀ = 58 μ
15.5 IN. CHAMBER - EXPERIMENTAL POINTS.
0 1 2 3 4 5 6 7 8 9 10 11 12 13 14 15 16
DISTANCE FROM INJECTOR (INCHES)

FIGURE 7

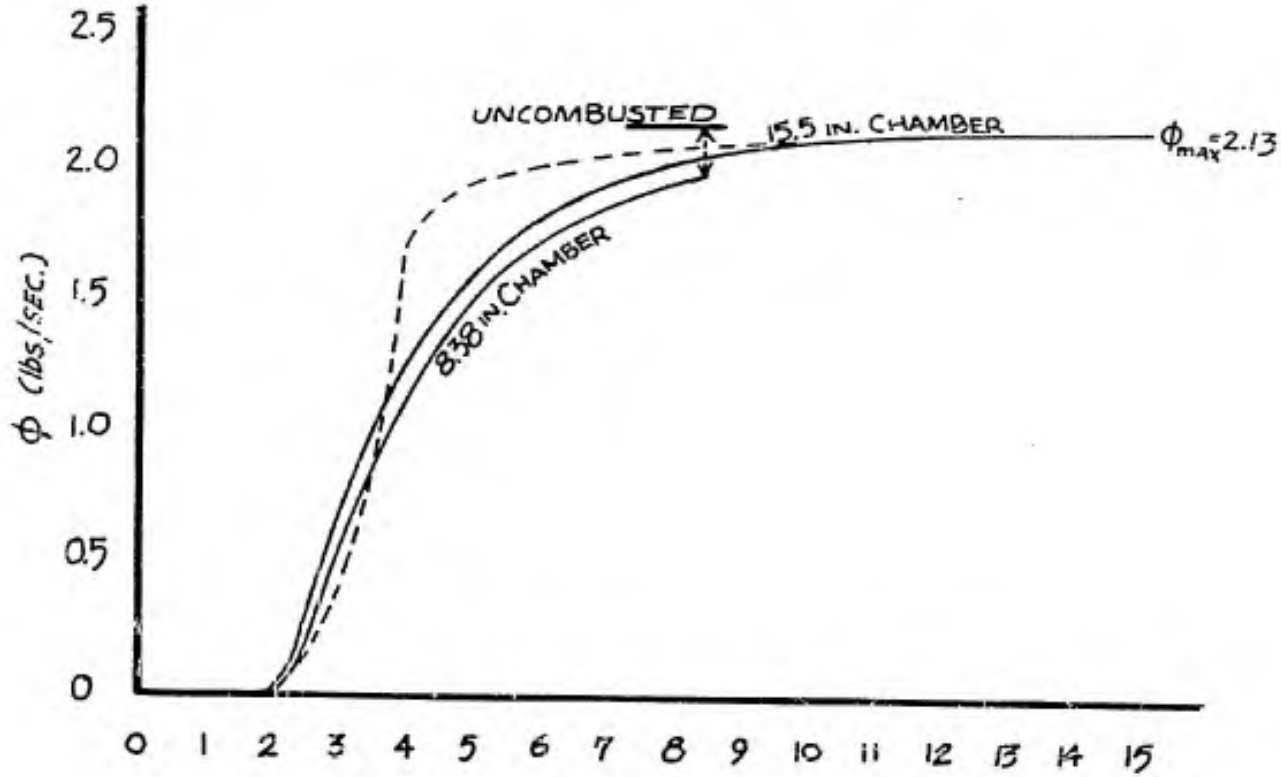
2.5
2.0
1.5
1.0
0.5
0
φ (lbs/sec.)
UNCOMBUSTED
15.5 IN. CHAMBER
ϕ_{max}=2.13
8.38 IN. CHAMBER
0 1 2 3 4 5 6 7 8 9 10 11 12 13 14 15
DISTANCE FROM INJECTOR (INCHES)

FIGURE 8

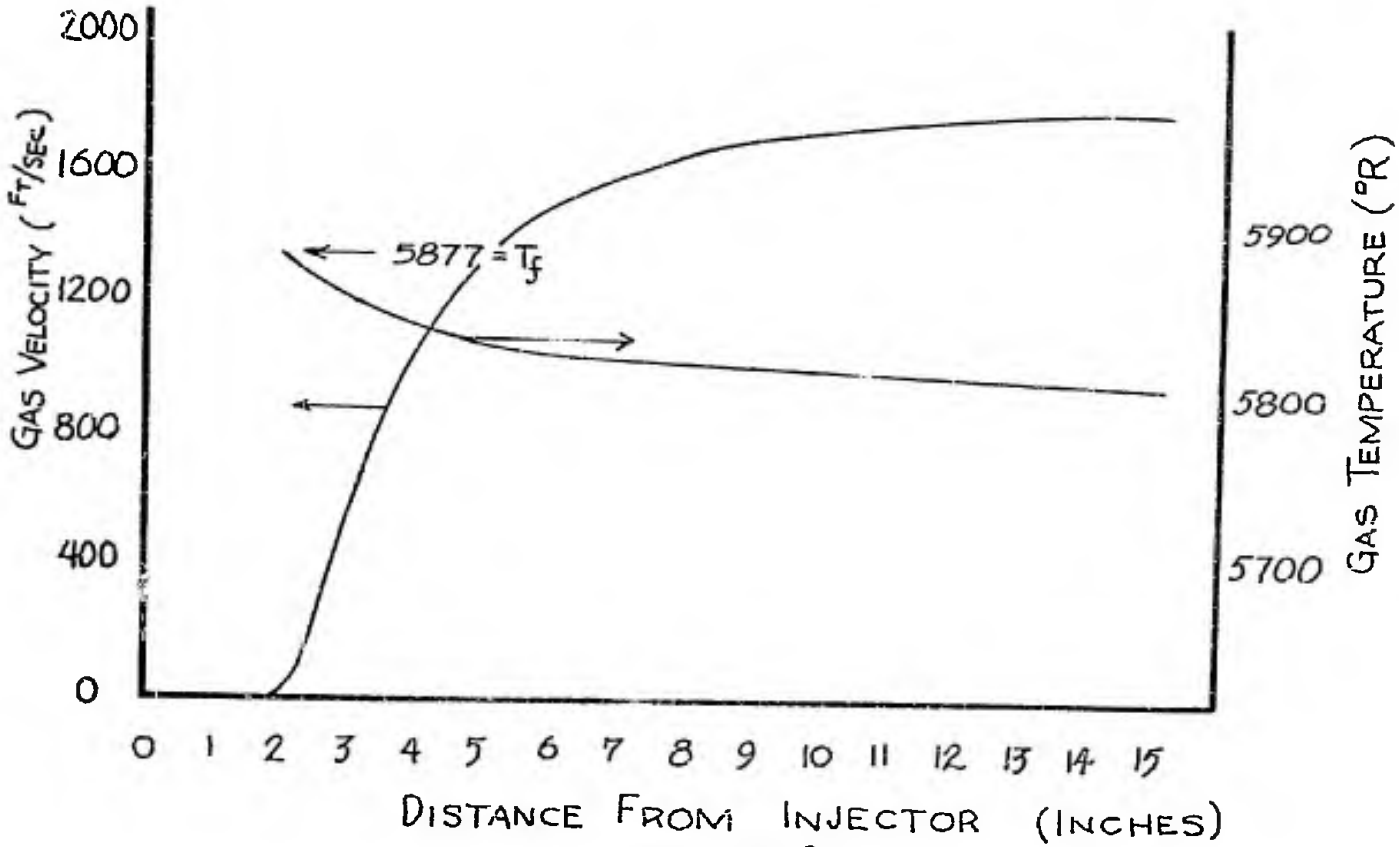
2000
1600
1200
800
400
0
GAS VELOCITY (FT/SEC)
5877 = T_f
5900
5800
5700
GAS TEMPERATURE (°R)
0 1 2 3 4 5 6 7 8 9 10 11 12 13 14 15
DISTANCE FROM INJECTOR (INCHES)

FIGURE 9

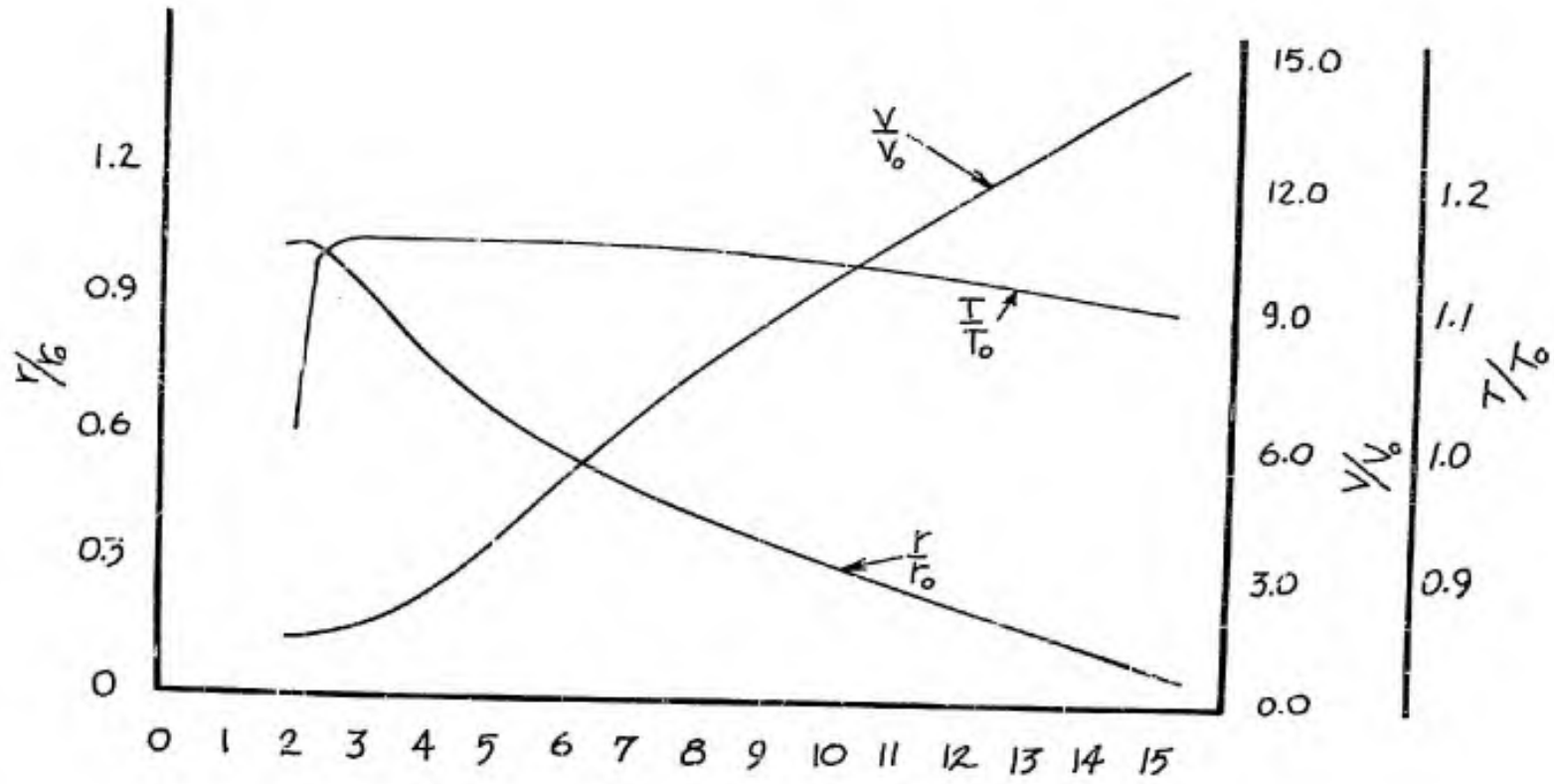
1.2
0.9
0.6
0.3
0
r/r₀
V/V₀
T/T₀
15.0
12.0
9.0
6.0
3.0
0.0
1.2
1.1
1.0
0.9
0 1 2 3 4 5 6 7 8 9 10 11 12 13 14 15
DISTANCE FROM INJECTOR (INCHES)

FIGURE 10

UNCLASSIFIED